ADVANCED FUNCTIONAL MATERIALS
www.afm-journal.de

A Flexible and Electrically Conductive Liquid Metal Adhesive for Hybrid Electronic Integration

*Tyler A. Pozarycki, Wuzhou Zu, Brittan T. Wilcox, and Michael D. Bartlett**

Electrical and mechanical integration approaches are essential for emerging hybrid electronics that must robustly bond rigid electrical components with flexible circuits and substrates. However, flexible polymeric substrates and circuits cannot withstand the high temperatures used in traditional electronic processing. This constraint requires new strategies to create flexible materials that simultaneously achieve high electrical conductivity, strong adhesion, and processibility at low temperature. Here, an electrically conductive adhesive is introduced that is flexible, electrically conductive (up to 3.25×10^5 S m^{-1}) without sintering or high temperature post-processing, and strongly adhesive to various materials common to flexible and stretchable circuits (fracture energy 350 $< G_c <$ 700 J m^{-2}). This is achieved through a multiphase soft composite consisting of an elastomeric and adhesive epoxy network with dispersed liquid metal droplets that are bridged by silver flakes, which form a flexible and conductive percolated network. These inks can be processed through masked deposition and direct ink writing at room temperature. This enables soft conductive wiring and robust integration of rigid components onto flexible substrates to create hybrid electronics for emerging applications in soft electronics, soft robotics, and multifunctional systems.

1. Introduction

Flexible and hybrid circuits are an emerging technology with promising applications in modern electronics,[1–5] wearable and implantable health-monitoring devices,[6–15] and soft robotics.[16–19] Traditionally, electronic components have been soldered to rigid printed circuit boards (PCBs) either manually or through the use of automated systems such as reflow ovens and wave solder machines. However, when creating hybrid electronics consisting of flexible or stretchable substrates with rigid, functional components, utilizing these techniques to attach the components to the flexible substrates is a challenge.[20–22] For example, typical tin-lead solders have melting temperatures that are often in excess of the glass transition temperatures of polymeric substrates commonly used for flexible circuits, which can lead to thermal expansion or damage.[23] Low-temperature solders, which incorporate low-melting point metals such as bismuth and indium, can be used to prevent damage to substrates; however, a vast majority of solder alloys, regardless of their melting temperature, tend to be brittle in their solid state. Consequently, bending, twisting, or other deformations inherent to flexible or soft systems can cause fracture or delamination of the solder and components.[22,24,25] As a result, there is an increasing need for materials that can be processed at room temperature while also having high flexibility, electrical conductivity, and strong adhesion, as these properties are essential to component integration in flexible and hybrid electronic systems.

Polymer-based electrically conductive adhesives (ECAs) are another option for interconnects in deformable systems.[26–30] However, their fabrication and integration into these systems have proven to be difficult. For example, intrinsically conductive polymers have been used as ECAs, but these typically have lower values of conductivity ($10^2 < \sigma < 10^3$ S m^{-1}) and poor adhesion strength,[31,32] and various mechanical and chemical processes are required to enhance these properties.[33–37] Another method to enhance electrical conductivity and adhesion is to put fillers such as conductive ceramics, carbon-based fillers, and metals into naturally adhesive polymers such as epoxies.[38–42] However, most epoxies do not have the desired mechanical properties to act as a flexible interconnect, as they are typically rigid ($E \geqslant 1$ GPa)[43,44] and thus do not easily interface with flexible substrates. Additionally, rigid fillers can further increase the modulus of the composite system, which is detrimental for deformable applications. It therefore remains a challenge to create materials with optimal combinations of flexibility, conductivity, and adhesion for flexible and hybrid electronic systems.

Here, we present a highly flexible and electrically conductive adhesive for hybrid electronics that is conductive as-prepared

T. A. Pozarycki, W. Zu, B. T. Wilcox, M. D. Bartlett
Mechanical Engineering
Soft Materials and Structures Lab
Virginia Tech, Blacksburg, VA 24061, USA
E-mail: mbartlett@vt.edu
M. D. Bartlett
Macromolecules Innovation Institute
Virginia Tech, Blacksburg, VA 24061, USA

The ORCID identification number(s) for the author(s) of this article can be found under https://doi.org/10.1002/adfm.202313567

DOI: 10.1002/adfm.202313567

without sintering or high-temperature post-processing, and adheres to a variety of materials without surface modification. These characteristics are enabled through the incorporation and interaction of liquid metal (LM) droplets (eutectic gallium-indium (EGaIn)) and silver (Ag) flakes in a flexible and adhesive epoxy matrix (**Figure** 1a(i–iv)). Therefore, the composite material is termed E-CASE (electrically conductive adhesive with silver and EGaIn). In the uncured state, the material can be deposited through various techniques, including direct ink write (DIW) (Figure 1b(i)) or stencil printing (Figure 1c(i)) onto flexible substrates like polyethylene terephthalate (PET), flex circuit (etched copper traces on polyimide), and stretchable elastomeric substrates like styrene-isoprene-styrene (SIS) copolymer (Figure 1d(i)). Rigid functional components can then be integrated, and the ink is cured between room temperature and 100 °C, at which point the material robustly adheres to the substrate and functional components. This allows for its use as both soft wiring as well as an interconnect for contact pads. The assemblies are capable of maintaining a very low bending radius, as demonstrated by wrapping the flexible circuits with an LED around a metal rod with a 2 mm diameter with continuous LED function (Figure 1b,c(ii,iii)). The assemblies are also applicable for stretchable electronics, as demonstrated by stretching an E-CASE integrated LED to ≈400% strain (Figure 1d(ii,iii)). By varying the silver content within E-CASE, the electrical and adhesive properties can be tuned. With a lower loading of Ag, the adhesive has an electrical conductivity of 3.75×10^4 S m^{-1} and a fracture energy of up to 675 J m^{-2}, while at a higher loading, it has a conductivity of 3.25×10^5 S m^{-1} with a fracture energy of up to 380 J m^{-2} (Figure 1d,e). The combination of adhesion, flexibility, low temperature processing, and inherent electrical conductivity is exceptional compared to other epoxy and LM-based composites.[45–55] These results demonstrate the utility of multiphase soft composites for the mechanical and electrical integration of hybrid electronics.

2. Results and Discussion

2.1. Electrically Conductive Adhesives

E-CASE consists of a flexible epoxy matrix ($E \approx 1$ MPa, Figure S1a, Supporting Information) which contains dispersed droplets of room-temperature LM (EGaIn) and Ag flakes. The LM and Ag were chosen as fillers due to their contrasting yet synergistic properties. EGaIn has a low viscosity and forms an oxide shell,[56,57] which makes it mechanically soft and typically creates an electrically insulating composite when dispersed in a polymer matrix,[58] while Ag flakes are rigid and have been shown to have the most electrically conductive geometry compared to micro and nanoparticles, especially in deformable applications.[59–61] In this work, the electrical and mechanical performance of two distinct formulations of the conductive adhesive were evaluated. The compositions focus on a lower loading of Ag with an emphasis on LM, to leverage the soft nature of the LM inclusions to maintain high flexibility. The first composition has a total filler loading of 68 vol%, composed of 58.8 vol% LM and 9.2 vol% Ag to achieve low bulk resistance; the second has a total filler loading of 73 vol%, with 50 vol% LM and 23 vol% Ag to further increase electrical conductivity. The two compositions are denoted herein as low Ag and high Ag, respectively.

2.2. Microstructure and Electrical Conductivity

To evaluate the microstructure of the material, optical microscopy, 3D profilometry, and SEM imaging were utilized. Upon measuring the 3D profile of a stencil-deposited trace, it was observed that the cross-section has a generally rectangular shape (**Figure** 2a). A closer examination of the top surface under SEM reveals an abundance of micron-size Ag flakes (Figure 2b). However, there was a lack of observable LM droplets. This is due to the very low viscosity and low density of the uncured epoxy matrix in comparison to the LM droplets. Since EGaIn has a higher density, the droplets settle into the bulk during fabrication (see Experimental Section) and thus are not seen on the surface after curing. Ag is also seen throughout the bulk; however, due to EGaIn's high surface tension,[62] oxide shell, and low mixing speeds during fabrication, the Ag shrouds the droplets (Figure 2c). This morphology aids in the creation of conductive pathways throughout the composite.[61,63] As shown in Figure 2d, if the LM is removed from the system but the amount of Ag remains the same, the low Ag formulation is no longer conductive, and the high Ag formulation is an order of magnitude less conductive. Additionally, in formulations where LM is the only filler and the total filler content is held constant, there is no electrical conductivity as fabricated, which is consistent with prior results of highly filled LM composites.[64] These results highlight the importance of the LM as a conformal and spatial filler in this biphasic composite.

The electrical behavior of the material was analyzed by quantifying resistance-length and current–voltage characteristics. It is found that the resistance-length behavior follows a positive linear trend, which is typical of conductors (Figure 2e). Linear least-squares fits predict an increase of ≈0.75 Ω per cm of trace length for the low Ag formulation and ≈0.06 Ω per cm for the high Ag formulation. It should be noted that, for high Ag, all resistance values up to $d = 40$ mm are less than 0.25 Ω with $d = 10$ mm in particular having an extremely low value of 0.09 Ω. Additionally, the low Ag formulation has a sub-ohm resistance of 0.55 Ω at $d = 10$ mm. Figure 2f shows the current–voltage behavior up to 0.5 V of applied voltage at a probing distance of $d = 40$ mm. Low Ag demonstrates less current draw per voltage applied compared to high Ag, with maximum current draw for each around 0.25 and 2.0 A, respectively. These results support the use of the E-CASE as both an effective material for solder-like connections as well as a soft wiring for flexible PCBs.

Common components of interest for hybrid electronics are rigid surface-mount components. These packages are typically on the scale of millimeters and include components such as pulse oximeters, time of flight sensors or heart-rate monitors for wearable technologies. To verify the feasibility of E-CASE on this type of package size, a set of connection pads with dimensions of 0.7 × 0.3 mm and a spacing of 0.4 mm were designed in addition to a custom circuit pattern with a close spacing as small as 220 µm for the 1005 metric surface mount device (SMD) package size (Figures S2 and S3, Supporting Information). These were stencil printed using masks fabricated with a CO_2 laser cutter. To further improve the resolution of E-CASE patterning,

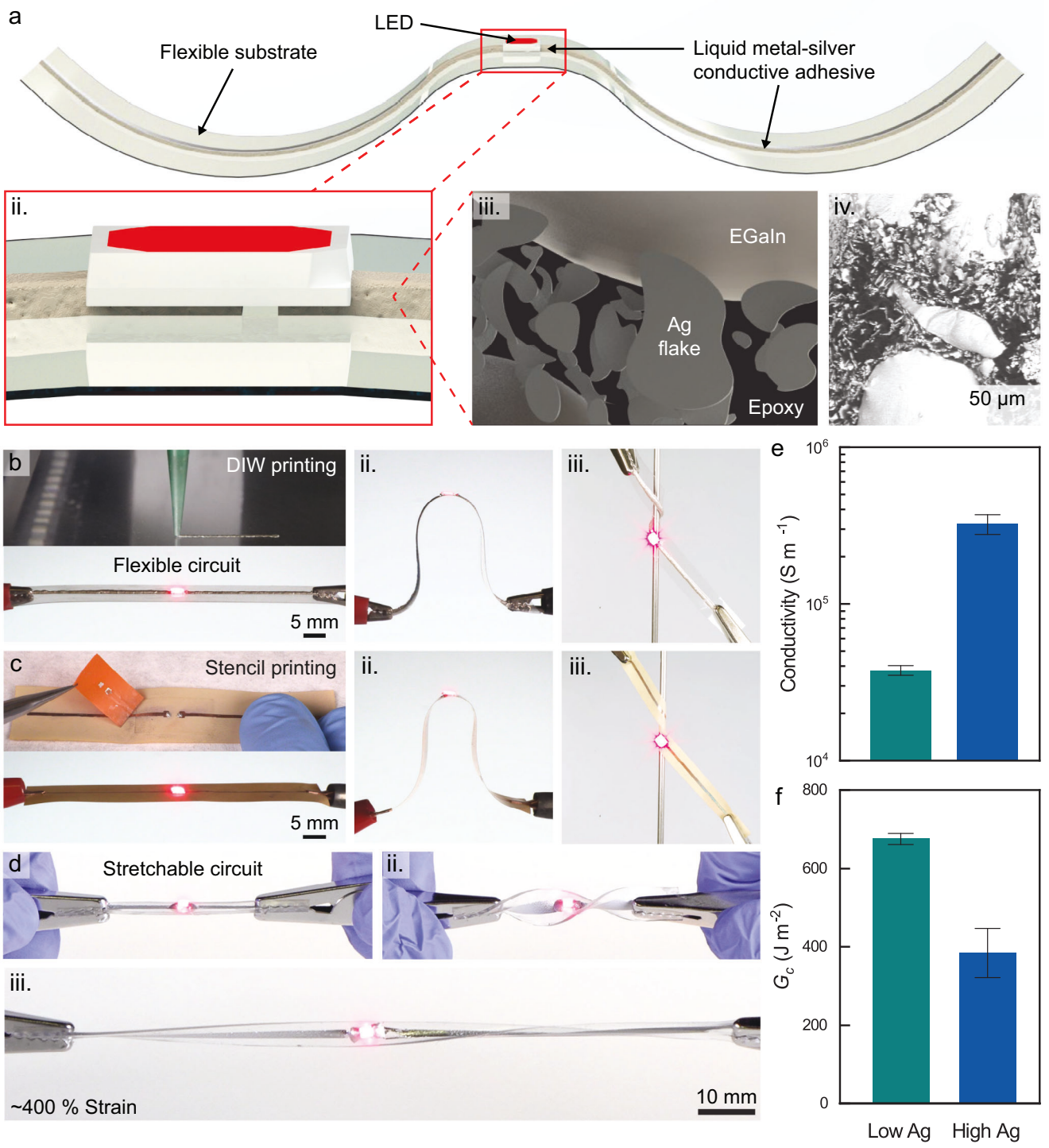

Figure 1. Highly flexible, electrically conductive adhesive. a) Schematics showing the implementation of E-CASE for traces and integration with a functional component (LED) and the composite microstructure. b) LED E-CASE assembly and demonstration of the flexural capabilities on PET with soft wiring; c) on flex circuit with pad interconnects; and d) stretchable capabilities on SIS elastomer with LM wiring for a stretchable circuit ($\epsilon = 400\%$). e) Electrical conductivity data for two material formulations. Error bars represent the s.d. for $n = 9$ based on cross-sectional area. f) Adhesion data (fracture energy G_c under peel) for the two material formulations. Error bars represent the s.d. for $n = 3$.

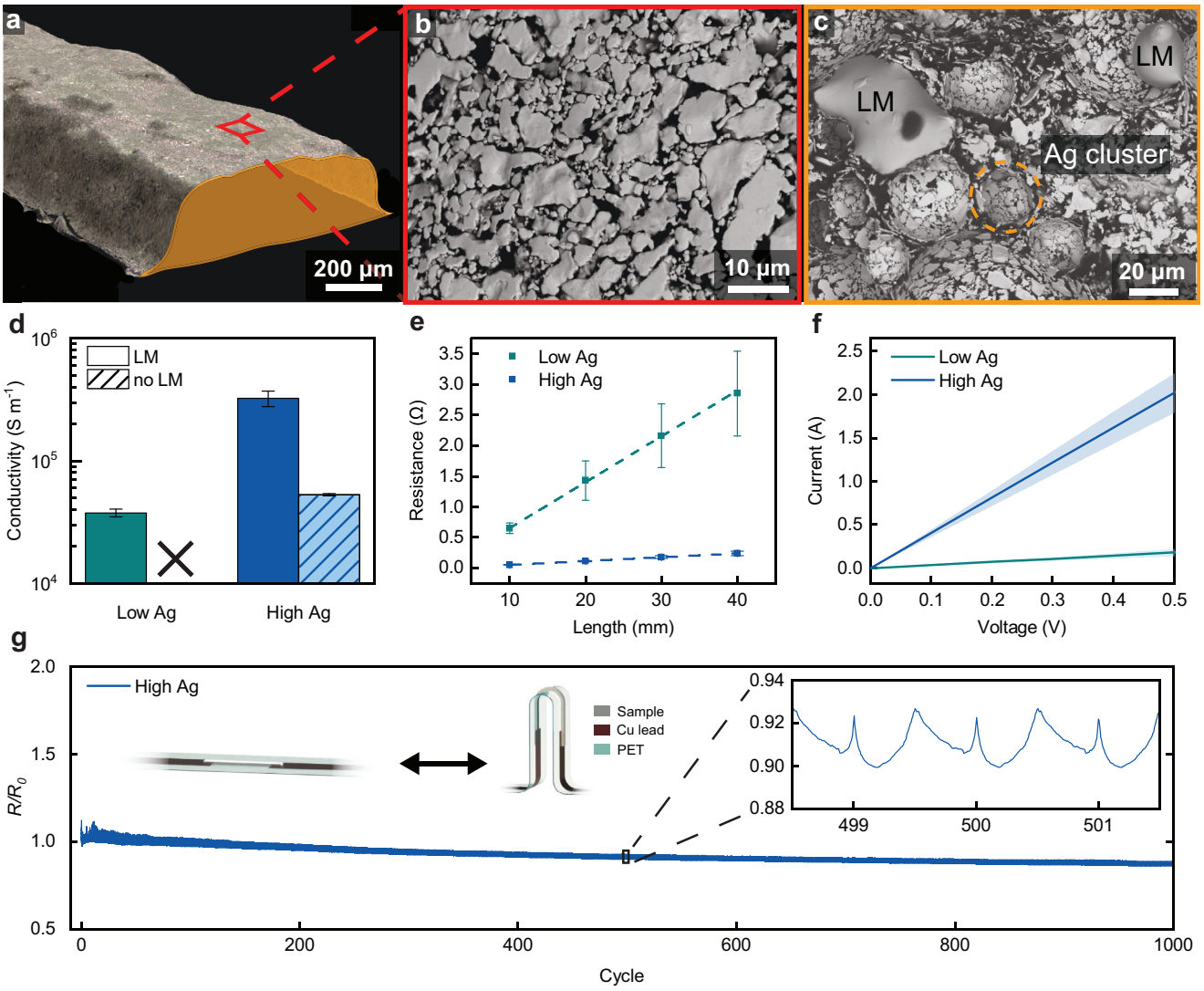

Figure 2. Conductive trace microstructure and electrical characterization. a) 3D optical rendering of a conductive trace with a width of 1 mm and a height of ≈480 µm. b) SEM image of trace surface microstructure. c) SEM image of trace cross-sectional area showing clusters of silver flakes and LM droplets. d) Conductivity of the E-CASE composite with and without LM. Error bars represent the s.d. for $n = 9$ measurements based on cross-sectional area. e) Resistance versus length measurements across conductive traces and corresponding linear fits. Error bars represent the s.d. for $n = 3$ measurements. f) Current–voltage curves up to 0.5 V for the conductive traces. Shaded regions represent the s.d. for $n = 3$ measurements. g) Normalized resistance of a conductive trace with high Ag loading under cyclic bending with the inset detailing cyclic behavior.

higher-resolution masks could be used. Additionally, recent work has shown promising high-resolution methods such as photopatterning of LM materials,[55] which is another pathway for improved resolution.

In flexible electronics applications, E-CASE needs to be conductive under repeated bending cycles. Cyclic bending was performed by bending a trace of high Ag E-CASE on a PET substrate to 1000 cycles (see Figure S4, Supporting Information, for experimental details). It is noted that E-CASE still maintains conformal contact with the electrode after the cyclic test. During the test, the traces remain conductive as the cycle count increases, eventually nearing a plateau (Figure 2g). For each individual cycle, it was found that the resistance shows minimal increases when bending and slight decreases when flattening. The cycles also contain a small peak near the end; this phenomenon has also been seen in carbon nanotube-epoxy composites, attributed to temporary changes in contact angle of nearby inclusions during repeated deformation.[65] The slight overall decrease in bulk resistance after 1000 cycles is likely a result of high bending stresses at the top peak causing the oxide layers on LM droplets near the center of the trace to rupture, which in turn allows for the LM to coalesce with surrounding Ag flakes and create additional conductive pathways.[61,66] Additionally, negligible differences in the bending rigidity of the flexible substrate were found with and without E-CASE (Figure S1b, Supporting Information), showing that E-CASE is highly compatible with the mechanical characteristics of the flexible substrates and can be implemented without impeding flexibility (Figure S5, Supporting Information).

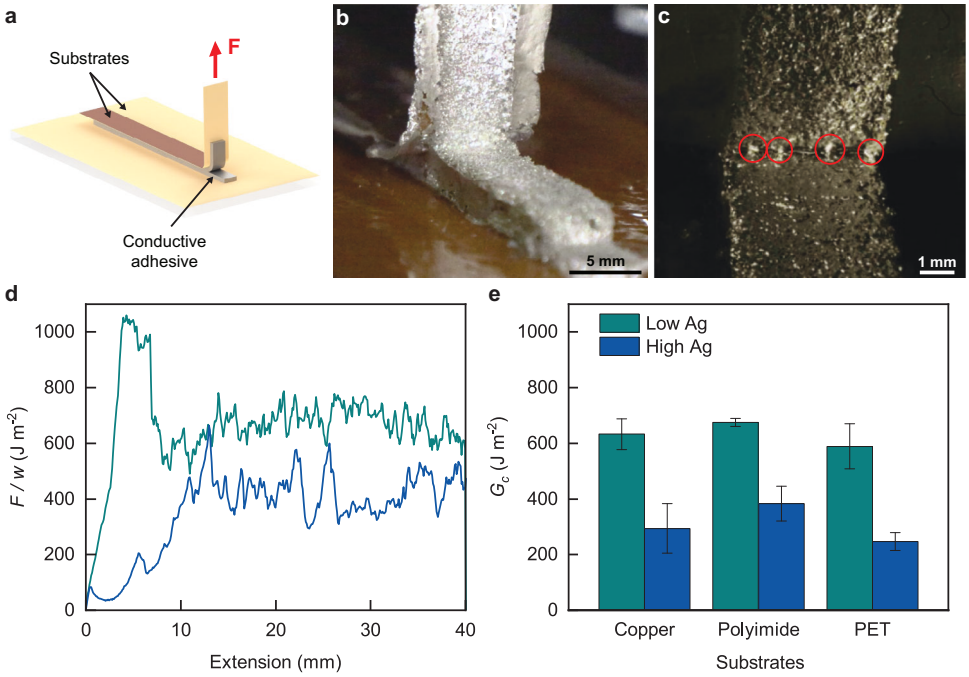

Figure 3. Adhesion characterization of conductive adhesive. a) Schematic of the 90° peel test of conductive adhesive. b) Isometric view of peel test showing steady-state cohesive fracture. c) Close-up front view of crack front during peeling with encircled bridging LM droplets. d) Representative peel curves on a polyimide substrate with $w = 5$ mm and e) G_c values obtained with both formulations on different substrates.

2.3. Adhesion Mechanism and Characteristics

Strong adhesion is critical for integration in flexible applications, where the material must be able to withstand stresses induced by bending and twisting near integrated components. To analyze the adhesion performance of E-CASE, 90° peel tests were utilized in which the material was cast between a rigid bottom substrate and a flexible top substrate (**Figure 3a**). Copper, polyimide, and PET were chosen as substrate materials due to their common use in hybrid electronic applications. At the onset of peeling, the crack front moves from the center of the thickness (pre-crack) towards the top substrate. Although the crack front propagated towards the interface, the material does not delaminate from the adherends. All samples exhibited cohesive fracture, as evidenced by a thin layer of material left on the adherend after testing. An interesting aspect of the material fracture was that LM droplets actively bridge the crack front during crack propagation (Figure 3b,c; Video S1, Supporting Information). However, no active liquid is left on the fracture surface after testing. Hence, the LM temporarily locates at the crack front, but then breaks apart and again becomes surrounded by Ag flakes on both fracture surfaces. Although crack bridging is a toughening mechanism observed in tough ceramics and fiber reinforced elastomer systems,[67,68] this liquid-bridging phenomenon has not been observed in other LM composite systems that undergo fracture or adhesion.[37,69,70] The bridging observed in these E-CASE composites likely arises due to the high inclusion content, where the cohesive failure drives liquid from the bulk material to the interface during crack propagation. Liquid–solid phase separation has been observed in self-healing polymers[71,72] and regions of high stress in swollen elastomers,[73,74] but these swollen elastomers are typically homogeneous upon mixing, while the E-CASE composites are heterogeneous. This unique mechanism represents a promising avenue for toughening in solid-liquid composites, especially in the context of multiphase composites where the solid-phase can act to encapsulate the liquid phase after the crack bridging is complete.

Figure 3d shows representative peel data for the fracture energy ($G_c = F/w$) of the system, where F is the peel force and w is the width of the sample.[75] Figure 3e shows a bar chart representation of G_c, where an average peel force has been taken across the plateau region. The low Ag formulation has greater values of G_c on all flexible substrates (up to ≈700 J m^{-2}) compared to its high Ag counterpart (up to ≈400 J m^{-2}). This is attributed to the high Ag formulation having less epoxy as a result of the higher overall filler content, which effectively decreases the tough epoxy between the inclusions. Furthermore, the values of G_c are found to be relatively similar on the copper, polyimide, and PET substrates within the same formulation. Additionally, we can utilize E-CASE on the transparent conductor indium tin oxide (ITO). Here, LEDs can be integrated with E-CASE for mechanical and electrical interfaces while achieving similar values of G_c compared to the other flexible substrates tested (Figure S5, Supporting Information). This is a result of the cohesive failure mechanism across all samples. In stark contrast to E-CASE, elastomer-based polydimethylsiloxane (PDMS)-conductive composites with the same composition of LM and Ag exhibit poor adhesion (Figure S6, Supporting Information). Given the strong adhesive properties of E-CASE paired with its high flexibility and conductivity, its integration into hybrid systems consisting of both rigid and flexible components is promising.

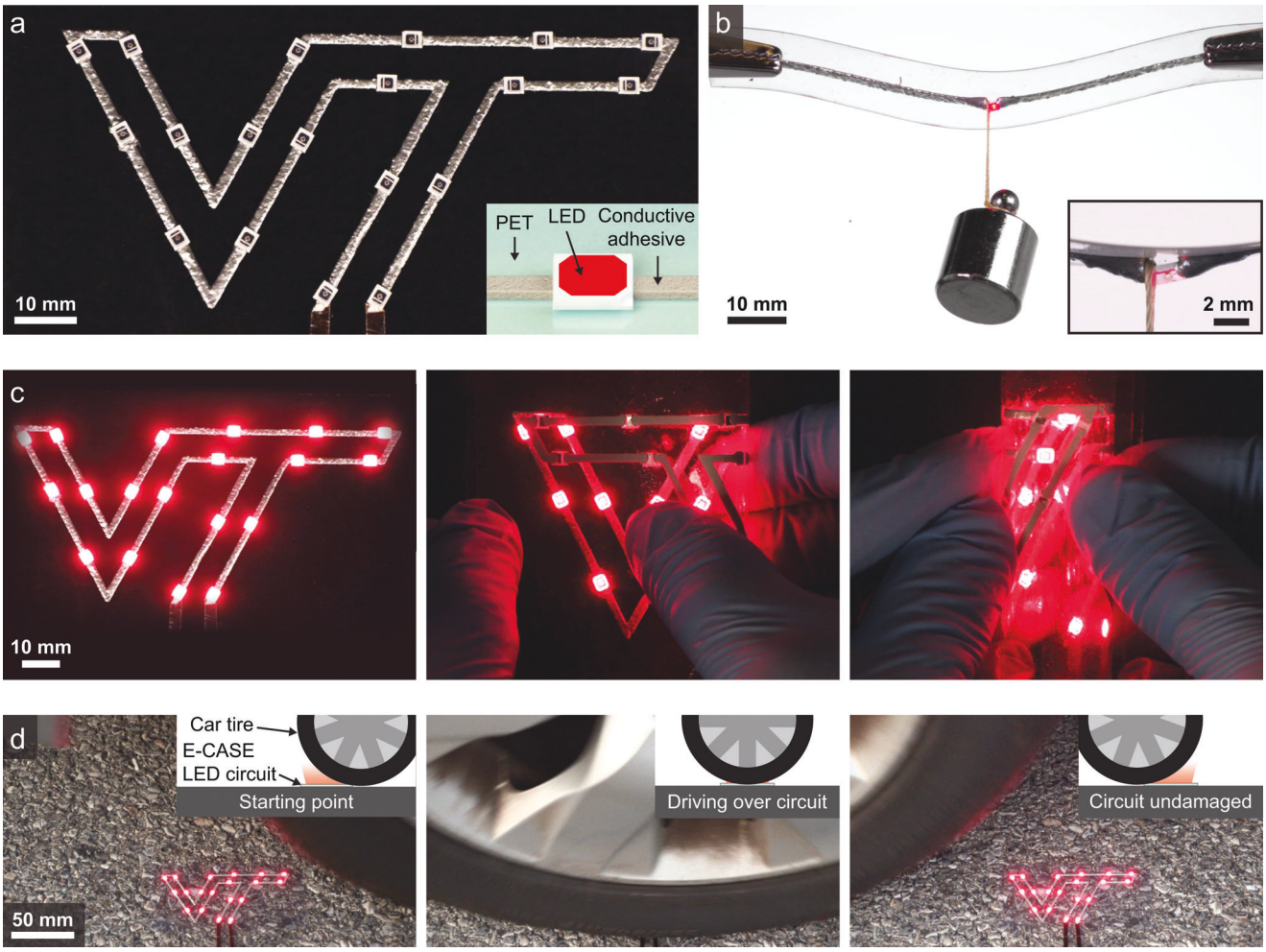

Figure 4. Robust hybrid electronics demonstration. a) Flexible electronic device with an inset schematic of an LED interfaced with the E-CASE adhesive on a PET substrate. b) LED adhered to PET with E-CASE, which supports a 20 g weight hanging from the LED. c) Folding the flexible device long-ways, and folding long-ways again. d) Timelapse with schematics showing the hybrid electronic device remaining functional after experiencing extreme stresses from being run over by a car. Registered Virginia Tech trademark printed with the approval of Virginia Tech Office of Licensing and Trademarks.

2.4. Robust Hybrid Electronics Integration

To demonstrate the feasibility and multifunctionality of the material in hybrid deformable systems, a flexible electronic device was created in which 19 LEDs were connected and interfaced with the low Ag E-CASE composite in series. The material was stencil-printed such that it forms the letters "VT" on a sheet of flexible, transparent PET (**Figure** 4a). These 19 LEDs are held securely by the adhesion of the E-CASE, as demonstrated by hanging a 20 g weight from a representative LED (Figure 4b). The device was folded long-ways twice, and no LEDs delaminate from the substrate or short during the process (Figure 4c). This highlights the multifunctionality of the E-CASE as a soft wire and electrically conductive adhesive, as well as its robustness to bending and creasing. As shown in Figure 4d, the powered circuit was then laid on pavement and subjected to extreme forces and pressure as a result of being driven over by a car. As this occurs, there is no delamination of the LEDs, nor does the circuit fail at any point. After the tire passes over the assembly, all 19 LEDs remain illuminated, and there were no signs of any shorts or broken conductive pathways on the circuit. This further shows the strong adhesive properties of the E-CASE composite as well as its ability to endure large amounts of stress while continuing to function. These results demonstrate the use of the E-CASE composite as both a soft wiring and a highly flexible interconnect for systems that incorporate both rigid and flexible functional components.

3. Conclusions

In this work, we introduced an electrically conductive adhesive through a multiphase soft composite that does not require sintering or high temperature post-processing, making it a strong candidate for hybrid electronics integration. The composite consists of liquid metal droplets bridged by silver flakes, which enable flexibility, electrical conductivity (up to 3.25×10^5 S m^{-1}) and strong adhesion (cohesive fracture energy $350 < G_c < 700$ J m^{-2}) to flexible circuit materials such as copper, polyimide, and PET. Across two material compositions, a trade-off is presented in which conductivity increases and adhesion decreases with greater Ag content. Specifically, increasing the amount of

Ag from 9.2 vol% to 23 vol% increases the conductivity by an order of magnitude (10^4 to 10^5 S m^{-1}) but decreases the fracture energy by about half (≈700 J m^{-2} to ≈350 J m^{-2}). As the material fractures, a unique liquid-bridging phenomenon was discovered in which LM spans the crack front across the top and bottom fracture surfaces. The unique combination of the material properties, including flexibility, conductivity, and adhesion are highlighted through the fabrication of a hybrid rigid-flexible system that can withstand tight bends and extreme pressure. These findings can inspire the future development of soft robotic and electronic systems, skin-mounted medical devices, and machines in which reliable mechanical and electrical integration of rigid and deformable components is critical to system function.

4. Experimental Section

Conductive Adhesive Fabrication: Low Ag (SF94, Ames Goldsmith Corporation) samples were fabricated by adding 58.8 vol% LM and 9.2 vol% Ag flakes to 32 vol% mixed, uncured flexible epoxy matrix (832FX, MG Chemicals) and hand-mixing until homogeneous. For high Ag samples, additional Ag was added to the low Ag mixture to increase the volume loading to 23.4 vol% and decrease the LM and epoxy to 50.2 vol% and 26.4 vol%, respectively. Approximately 20 wt% acetone was used to reduce viscosity and the solution was hand-mixed again. The LM was EGaIn, 3:1 mass ratio of gallium and indium.

Conductive Trace and Interconnect Fabrication: Stencils were fabricated by laser cutting masks 55 mm in length, 1 mm in width and ≈480 µm in height on a stencil mask (Blazer Orange Laser Mask, Johnson Plastics Plus, three layers). The stencils were placed onto a 125 µm-thick PET substrate and the conductive adhesive was deposited and leveled with a tongue depressor before removing the stencil mask layer by layer with tweezers. DIW prints were done by loading the paste into a syringe and then placing the syringe into a SDS-10 head on a Hyrel Engine SR 3D printer. The material was extruded onto 125 µm PET at 2000–2500 pulses per microliter and head speeds of 600–800 mm min^{-1}. LEDs were placed down using tweezers and assemblies were cured at 100 °C for 30 min.

Indentation Sample Fabrication: PDMS molds (Sylgard 184, Dow, 10:1 curing ratio) were fabricated in the shape of a hollow square with dimensions of 15 × 15 × 19 mm. Molds were affixed to an acrylic substrate using a thin layer of silicone adhesive (Sil-Poxy, Smooth-On), and the epoxy was deposited into the mold. A thin sheet of cured PDMS was laid on top of the mold to ensure a flat sample surface. Samples were cured at 100 °C for 1 h.

Peel Specimen Fabrication: PDMS molds (Sylgard 184, Dow, 10:1 curing ratio) were prepared by casting the uncured silicone into a large acrylic mold to create a stock sheet. The molds (75 × 5 mm with a 5 mm wall thickness) were laser-cut from the stock and cleaned thoroughly in a container of isopropyl alcohol floating in a sonication bath. Substrates (copper, polyimide, and PET) were affixed to a supporting acrylic substrate using VHB tape (3M). The molds were sealed to the bottom substrate by applying a thin layer of Sil-Poxy. Samples were cast into the molds, and another substrate (120 × 5 mm) was placed on top. Specimens were cured at room temperature overnight and then at 100 °C for 30 min. The molds were removed after curing and a 10 mm central pre-crack was cut into the material with a razor blade prior to testing.

Flexible Electronics Demonstration Fabrication: The circuit was fabricated by laser-cutting a stencil mask (two layers). 2.5-mm breaks in the lines were periodically integrated for LEDs. The stencil was placed onto PET and the conductive adhesive was manually deposited and leveled before removing the mask. LEDs were placed down using tweezers and the completed assembly was cured at 100 °C for 30 min. After curing, the circuit was spray-coated with a thin layer of polyurethane (HumiSeal).

Mechanical and Adhesion Characterization: All mechanical data was obtained using an Instron 5944 universal testing system. The elastic modulus of the epoxy was measured using an indentation setup in which a hemispherical indenter (N-BK7 half-ball lens, 3 mm diameter, Edmund Optics) indented to 1 mm below the surface of a 15 × 15 × 19 mm sample at 0.5 µm s^{-1}. Bending data were measured using a three-point bend setup with a span length of 2 cm. Substrates were 4 cm long by 1 cm wide. Substrate thicknesses were 125 µm for PET and 120 µm for copper on polyimide (H/1/1/0, Pyralux, DuPont). Adhesion fracture energy data were obtained from a 30 mm plateau region of the force-displacement curves of specimens 75 × 5 × 3.2 mm (length × width × thickness) under 90° peel at 1 mm s^{-1}.

Electrical Measurements: Resistance versus length data were obtained using a source measuring unit (Keithley 2460) with a four-probe setup. To minimize contact resistance, small drops of LM were dispensed onto the surface of the conductive trace at the points of interest and copper probes were used to make measurements. *IV* curves were obtained using the same setup described above, a step voltage from 0 to 0.5 V in intervals of 0.1 V was sent through conductive traces at a fixed probe distance of 40 mm. The electrical conductivity was obtained through the formula $\sigma = L/RA$, where L/R is the inverse of the obtained linear least-squares relationship, and A is an average cross-sectional area of a conductive trace.

Cyclic resistance samples were made using the methods described in the fabrication section. Conductive traces with dimensions of 20 mm × 1 mm × 480 µm were stencil-deposited on 125 µm-thick PET atop extended copper leads (double-sided conductive copper foil tape, 3 mm width, Uxcell). The ends of the sample were secured with acrylic clamps onto a custom fixture with an integrated linear actuator and stepper motor (SY57STH56-2006A, Pololu). The motor was connected to an Arduino Uno/Adafruit Motorshield V2 stack, which was programmed using MATLAB to displace one clamp back and forth between a fixture separation of 35 and 17.5 mm over 1000 cycles. Resulting electrical data was obtained by connecting the extended copper leads on the sample to a source measuring unit (Keithley 2460) with alligator clips.

Microscopy and Profilometry: Optical images and profiles were obtained on a 3D profiler (Keyence VK-X3000) using white light at 5× magnification and a laser at 10× magnification. Cross-sectional area measurements were calculated using a slicing tool across the trace and manually adjusting the boundaries of the region to be considered. The micro-level particle analysis was performed on an analytical scanning electron microscope (SEM) using a Schottky field emission (FEG) electron source (JEOL IT-500HR). The scanning mode was set to backscattered electrons with an accelerating voltage of 15 kV.

Statistical Analysis: The meaning of all error bars was described within the captions of the corresponding figures. Statistical analysis was done using the computer program Origin Pro.

Supporting Information

Supporting Information is available from the Wiley Online Library or from the author.

Acknowledgements

The authors acknowledge support from the Office of Naval Research Young Investigator Program (YIP) (N000142112699), NSF (No. CMMI-2054409), and the Institute for Critical Technology and Applied Science (ICTAS) at Virginia Tech. This work used shared facilities at the Materials Characterization Lab and Nanoscale Characterization and Fabrication Laboratory, which are funded and managed by Virginia Tech's Institute for Critical Technology and Applied Science. Additional support was provided by the Virginia Tech National Center for Earth and Environmental Nanotechnology Infrastructure (NanoEarth), a member of the National Nanotechnology Coordinated Infrastructure (NNCI), supported by NSF (ECCS 1542100 and ECCS 2025151). The authors thank Dr. Dong Hae Ho for assistance with SEM imaging.

Conflict of Interest

The authors declare no conflict of interest.

Data Availability Statement

The data that support the findings of this study are available from the corresponding author upon reasonable request.

Keywords

adhesives, flexible electronics, liquid metals, soft composites, soft electronics

Received: October 31, 2023
Revised: December 20, 2023
Published online:

[1] D.-H. Kim, N. Lu, R. Ma, Y.-S. Kim, R.-H. Kim, S. Wang, J. Wu, S. M. Won, H. Tao, A. Islam, K. J. Yu, T. il Kim, R. Chowdhury, M. Ying, L. Xu, M. Li, H.-J. Chung, H. Keum, M. McCormick, P. Liu, Y.-W. Zhang, F. G. Omenetto, Y. Huang, T. Coleman, J. A. Rogers, *Science* **2011**, *333*, 838.
[2] N. Ilyas, A. Cook, C. E. Tabor, *Adv. Mater. Interfaces* **2017**, *4*, 1700141.
[3] B. H. Kim, F. Liu, Y. Yu, H. Jang, Z. Xie, K. Li, J. Lee, J. Y. Jeong, A. Ryu, Y. Lee, D. H. Kim, X. Wang, K. Lee, J. Y. Lee, S. M. Won, N. Oh, J. Kim, J. Y. Kim, S.-J. Jeong, K.-I. Jang, S. Lee, Y. Huang, Y. Zhang, J. A. Rogers, *Adv. Funct. Mater.* **2018**, *28*, 1803149.
[4] C. A. Silva, J. Lv, L. Yin, I. Jeerapan, G. Innocenzi, F. Soto, Y.-G. Ha, J. Wang, *Adv. Funct. Mater.* **2020**, *30*, 2002041.
[5] A. R. Jayakrishnan, A. Kumar, S. Druvakumar, R. John, M. Sudeesh, V. S. Puli, J. P. Silva, M. J. Gomes, K. C. Sekhar, *J. Mater. Chem. C* **2023**, *11*, 827.
[6] A. Santorelli, E. Porter, E. Kang, T. Piske, M. Popović, J. D. Schwartz, *IEEE Trans. Instrum. Meas.* **2015**, *64*, 2986.
[7] M. D. Bartlett, E. J. Markvicka, C. Majidi, *Adv. Funct. Mater.* **2016**, *26*, 8496.
[8] M. H. Malakooti, N. Kazem, J. Yan, C. Pan, E. J. Markvicka, K. Matyjaszewski, C. Majidi, *Adv. Funct. Mater.* **2019**, *29*, 1906098.
[9] H. Yuk, B. Lu, X. Zhao, *Chem. Soc. Rev.* **2019**, *48*, 1642.
[10] Y. Chen, Y. Zhang, Z. Liang, Y. Cao, Z. Han, X. Feng, *npj Flexible Electron.* **2020**, *4*, 2.
[11] S. Zhang, A. Chhetry, M. A. Zahed, S. Sharma, C. Park, S. Yoon, J. Y. Park, *npj Flexible Electron.* **2022**, *6*, 11.
[12] H.-P. Phan, *Micromachines* **2021**, *12*, 157.
[13] I. Heck, W. Lu, Z. Wang, X. Zhang, T. Adak, T. Cu, C. Crumley, Y. Zhang, X. S. Wang, *Adv. Mater. Technol.* **2023**, *8*, 2200821.
[14] S. M. McDonald, Q. Yang, Y.-H. Hsu, S. P. Nikam, Z. Hu, Z. Wang, D. Asheghali, T. Yen, A. V. Dobrynin, J. A. Rogers, M. L. Becker, *Nat. Commun.* **2023**, *14*, 7299.
[15] Y. Xu, Y. Su, X. Xu, B. Arends, G. Zhao, D. N. Ackerman, H. Huang, S. P. Reid, J. L. Santarpia, C. Kim, Z. Chen, S. Mahmoud, Y. Ling, A. Brown, Q. Chen, G. Huang, J. Xie, Z. Yan, *Sci. Adv.* **2023**, *9*, eadf0575.
[16] E. J. Markvicka, M. D. Bartlett, X. Huang, C. Majidi, *Nat. Mater.* **2018**, *17*, 618.
[17] Y. Xu, Q. Fei, M. Page, G. Zhao, Y. Ling, D. Chen, Z. Yan, *Nano Res.* **2021**, *14*, 3033.
[18] Y. Han, L.-E. Simonsen, M. H. Malakooti, *Adv. Energy Mater.* **2022**, *12*, 2201413.
[19] S. Shu, Z. Wang, P. Chen, J. Zhong, W. Tang, Z. L. Wang, *Adv. Mater.* **2023**, *35*, 2211385.
[20] M. T. I. Molla, S. Goodman, N. Schleif, M. E. Berglund, C. Zacharias, C. Compton, L. E. Dunne, in *Proceedings of the 2017 ACM International Symposium on Wearable Computers*, Association for Computing Machinery, New York, NY **2017**, pp. 18–25.
[21] X. Li, H. Andersson, J. Sidén, T. Schön, *Flexible Printed Electron.* **2018**, *3*, 015003.
[22] A. Martin, B. S. Chang, Z. Martin, D. Paramanik, C. Frankiewicz, S. Kundu, I. D. Tevis, M. Thuo, *Adv. Funct. Mater.* **2019**, *29*, 1903687.
[23] V. Kasi, A. Zareei, S. Gopalakrishnan, A. M. Alcaraz, S. Joshi, B. Arfaei, R. Rahimi, *Advanced Electronic Materials* **2023**, *9*, 2201012.
[24] X. Chen, Y. Lin, X. Liu, G.-Q. Lu, *Eng. Fract. Mech.* **2005**, *72*, 2628.
[25] Y.-H. Ko, M.-S. Kim, J. Bang, T.-S. Kim, C.-W. Lee, *J. Electron. Mater.* **2015**, *44*, 2458.
[26] R. Zhang, W. Lin, K. Lawrence, C. Wong, *Int. J. Adhes. Adhes.* **2010**, *30*, 403.
[27] Y. Ko, J. Oh, K. T. Park, S. Kim, W. Huh, B. J. Sung, J. A. Lim, S.-S. Lee, H. Kim, *ACS Appl. Mater. Interfaces* **2019**, *11*, 37043.
[28] J. Dou, L. Tang, L. Mou, R. Zhang, X. Jiang, *Compos. Sci. Technol.* **2020**, *197*, 108237.
[29] Y. Wang, Y. Yu, J. Guo, Z. Zhang, X. Zhang, Y. Zhao, *Adv. Funct. Mater.* **2020**, *30*, 2000151.
[30] K. George, A. Thomas, N. Shajimon, J. Joseph, R. Paul, *Int. J. Res. Appl. Sci. Eng. Technol* **2021**, *9*, 440.
[31] Y. Liu, J. Liu, S. Chen, T. Lei, Y. Kim, S. Niu, H. Wang, X. Wang, A. M. Foudeh, J. B.-H. Tok, Z. Bao, *Nat. Biomed. Eng.* **2019**, *3*, 58.
[32] A. Inoue, H. Yuk, B. Lu, X. Zhao, *Sci. Adv.* **2020**, *6*, eaay5394.
[33] C. J. Thrasher, Z. J. Farrell, N. J. Morris, C. L. Willey, C. E. Tabor, *Adv. Mater.* **2019**, *31*, 1903864.
[34] H. Yuk, B. Lu, S. Lin, K. Qu, J. Xu, J. Luo, X. Zhao, *Nat. Commun.* **2020**, *11*, 1604.
[35] S. Liu, D. S. Shah, R. Kramer-Bottiglio, *Nat. Mater.* **2021**, *20*, 851.
[36] P. Tan, H. Wang, F. Xiao, X. Lu, W. Shang, X. Deng, H. Song, Z. Xu, J. Cao, T. Gan, B. Wang, X. Zhou, *Nat. Commun.* **2022**, *13*, 358.
[37] T. A. Pozarycki, D. Hwang, E. J. Barron III, B. T. Wilcox, R. Tutika, M. D. Bartlett, *Small* **2022**, *18*, 2203700.
[38] R. Aradhana, S. Mohanty, S. K. Nayak, *Int. J. Adhes. Adhes.* **2020**, *99*, 102596.
[39] K. Chan, M. Mariatti, Z. Lockman, L. Sim, *J. Appl. Polym. Sci.* **2011**, *121*, 3145.
[40] S. Khairul Anuar, M. Mariatti, A. Azizan, N. Chee Mang, W. Tham, *J. Mater. Sci.: Mater. Electron.* **2011**, *22*, 757.
[41] X. Yang, W. He, S. Wang, G. Zhou, Y. Tang, *J. Mater. Sci.: Mater. Electron.* **2012**, *23*, 108.
[42] E. Sancaktar, L. Bai, *Polymers* **2011**, *3*, 427.
[43] F. H. Gojny, M. H. Wichmann, B. Fiedler, K. Schulte, *Compos. Sci. Technol.* **2005**, *65*, 2300.
[44] A. Gopinath, M. Senthilkumar, A. Babu, *Mater. Today: Proc.* **2018**, *5*, 20092.
[45] H. Wu, J. Liu, X. Wu, M. Ge, Y. Wang, G. Zhang, J. Jiang, *Int. J. Adhes. Adhes.* **2006**, *26*, 617.
[46] W.-T. Cheng, Y.-W. Chih, W.-T. Yeh, *Int. J. Adhes. Adhes.* **2007**, *27*, 236.
[47] D. Tee, M. Mariatti, A. Azizan, C. See, K. Chong, *Compos. Sci. Technol.* **2007**, *67*, 2584.
[48] Y. Guan, X. Chen, F. Li, H. Gao, *Int. J. Adhes. Adhes.* **2010**, *30*, 80.
[49] G. Johnsen, M. Knaapila, Ø. Martinsen, G. Helgesen, *Compos. Sci. Technol.* **2012**, *72*, 1841.
[50] B. C. Tee, C. Wang, R. Allen, Z. Bao, *Nat. Nanotechnol.* **2012**, *7*, 825.
[51] W. Qiao, H. Bao, X. Li, S. Jin, Z. Gu, *Int. J. Adhes. Adhes.* **2014**, *48*, 159.
[52] M. A. Rahim, F. Centurion, J. Han, R. Abbasi, M. Mayyas, J. Sun, M. J. Christoe, D. Esrafilzadeh, F.-M. Allioux, M. B. Ghasemian, J. Yang, J. Tang, T. Daeneke, S. Mettu, J. Zhang, M. H. Uddin, R. Jalili, K. Kalantar-Zadeh, *Adv. Funct. Mater.* **2021**, *31*, 2007336.
[53] G.-H. Lee, Y. R. Lee, H. Kim, D. A. Kwon, H. Kim, C. Yang, S. Q. Choi, S. Park, J.-W. Jeong, S. Park, *Nat. Commun.* **2022**, *13*, 2643.
[54] W. Lee, H. Kim, I. Kang, H. Park, J. Jung, H. Lee, H. Park, J. S. Park, J. M. Yuk, S. Ryu, J.-W. Jeong, J. Kang, *Science* **2022**, *378*, 637.

[55] G.-H. Lee, H. Kim, J. Lee, J.-Y. Bae, C. Yang, H. Kim, H. Kang, S. Q. Choi, S. Park, S.-K. Kang, J. Kang, Z. Bao, J.-W. Jeong, S. Park, *Mater. Today* **2023**, *67*, 84.
[56] M. D. Dickey, *Adv. Mater.* **2017**, *29*, 1606425.
[57] W. Kong, N. U. H. Shah, T. V. Neumann, M. H. Vong, P. Kotagama, M. D. Dickey, R. Y. Wang, K. Rykaczewski, *Soft Matter* **2020**, *16*, 5801.
[58] M. D. Bartlett, A. Fassler, N. Kazem, E. J. Markvicka, P. Mandal, C. Majidi, *Adv. Mater.* **2016**, *28*, 3726.
[59] J. Wang, G. Cai, S. Li, D. Gao, J. Xiong, P. S. Lee, *Adv. Mater.* **2018**, *30*, 1706157.
[60] A. Hajalilou, A. F. Silva, P. A. Lopes, E. Parvini, C. Majidi, M. Tavakoli, *Adv. Mater. Interfaces* **2022**, *9*, 2101913.
[61] W. Zu, Y. Ohm, M. R. Carneiro, M. Vinciguerra, M. Tavakoli, C. Majidi, *Adv. Mater. Technol.* **2022**, *7*, 2200534.
[62] R. W. Style, R. Tutika, J. Y. Kim, M. D. Bartlett, *Adv. Funct. Mater.* **2021**, *31*, 2005804.
[63] M. Reis Carneiro, C. Majidi, M. Tavakoli, *Adv. Funct. Mater.* **2023**, *33*, 2306453.
[64] R. Tutika, S. Kmiec, A. T. Haque, S. W. Martin, M. D. Bartlett, *ACS Appl. Mater. Interfaces* **2019**, *11*, 17873.
[65] Y. Wang, S. Wang, M. Li, Y. Gu, Z. Zhang, *Sens. Actuators, A* **2018**, *273*, 140.
[66] M. Tavakoli, M. H. Malakooti, H. Paisana, Y. Ohm, D. Green Marques, P. Alhais Lopes, A. P. Piedade, A. T. de Almeida, C. Majidi, *Adv. Mater.* **2018**, *30*, 1801852.
[67] R. O. Ritchie, *Nat. Mater.* **2011**, *10*, 817.
[68] D. R. King, T. L. Sun, Y. Huang, T. Kurokawa, T. Nonoyama, A. J. Crosby, J. P. Gong, *Mater. Horiz.* **2015**, *2*, 584.
[69] N. Kazem, M. D. Bartlett, C. Majidi, *Adv. Mater.* **2018**, *30*, 1706594.
[70] A. T. Haque, D. H. Ho, D. Hwang, R. Tutika, C. Lee, M. D. Bartlett, *Adv. Funct. Mater.* **2023**, 2304101, https://doi.org/10.1002/adfm.202304101.
[71] S. R. White, N. R. Sottos, P. H. Geubelle, J. S. Moore, M. R. Kessler, S. Sriram, E. N. Brown, S. Viswanathan, *Nature* **2001**, *409*, 794.
[72] Y. Zhao, Y. Ohm, J. Liao, Y. Luo, H.-Y. Cheng, P. Won, P. Roberts, M. R. Carneiro, M. F. Islam, J. H. Ahn, L. M. Walker, C. Majidi, *Nat. Electron.* **2023**, *6*, 206.
[73] Z. Cai, A. Skabeev, S. Morozova, J. T. Pham, *Commun. Mater.* **2021**, *2*, 21.
[74] L. Hauer, Z. Cai, A. Skabeev, D. Vollmer, J. T. Pham, *Phys. Rev. Lett.* **2023**, *130*, 058205.
[75] M. D. Bartlett, S. W. Case, A. J. Kinloch, D. A. Dillard, *Prog. Mater. Sci.* **2023**, 101086.